Optical and electrical properties of $BaSnO_3$ and In_2O_3 mixed transparent conductive films deposited by filtered cathodic vacuum arc technique at room temperature

Jian-Ke Yao(姚建可)[1,†] and Wen-Sen Zhong(钟文森)[2]

[1] *College of Materials & New Energy, South China Normal University, Shanwei* 516625, *China*
[2] *Blue Lake Optic-electronic Company, Huizhou* 516001, *China*

(Received 5 July 2022; revised manuscript received 19 August 2022; accepted manuscript online 26 August 2022)

For the crystalline temperature of $BaSnO_3$ (BTO) was above 650 °C, the transparent conductive BTO-based films were always deposited above this temperature on epitaxy substrates by pulsed laser deposition or molecular beam epitaxy till now which limited there application in low temperature device process. In the article, the microstructure, optical and electrical of BTO and In_2O_3 mixed transparent conductive $BaInSnO_x$ (BITO) film deposited by filtered cathodic vacuum arc technique (FCVA) on glass substrate at room temperature were firstly reported. The BITO film with thickness of 300 nm had mainly In_2O_3 polycrystalline phase, and minor polycrystalline BTO phase with (001), (011), (111), (002), (222) crystal faces which were first deposited at room temperature on amorphous glass. The transmittance was 70%–80% in the visible light region with linear refractive index of 1.94 and extinction coefficient of 0.004 at 550-nm wavelength. The basic optical properties included the real and imaginary parts, high frequency dielectric constants, the absorption coefficient, the Urbach energy, the indirect and direct band gaps, the oscillator and dispersion energies, the static refractive index and dielectric constant, the average oscillator wavelength, oscillator length strength, the linear and the third-order nonlinear optical susceptibilities, and the nonlinear refractive index were all calculated. The film was the n-type conductor with sheet resistance of 704.7 Ω/□, resistivity of 0.02 Ω·cm, mobility of 18.9 $cm^2/V{\cdot}s$, and carrier electron concentration of 1.6×10^{19} cm^{-3} at room temperature. The results suggested that the BITO film deposited by FCVA had potential application in transparent conductive films-based low temperature device process.

Keywords: $BaSnO_3$ and In_2O_3 mixed film, filtered cathodic vacuum arc deposition, transparent conductive films, microstructure, optical properties, electrical properties

PACS: 81.05.Hd, 78.66.–w, 73.61.–r **DOI:** 10.1088/1674-1056/ac8ce7

1. Introduction

$BaSnO_3$ (BTO)-based transparent conductive films have been exhaustively investigated until now for its wide bandgap with high room-temperature electron mobility and thermal stability.[1,2] For the crystalline temperature of BTO is above 650 °C,[3] the BTO-based films are always deposited above 650 °C on epitaxy substrate by pulsed laser deposition or molecular beam epitaxy till now to get high quality crystalline which limits their application in low temperature device.

The filtered cathodic vacuum arc (FCVA) technique is an attractive thin film deposition method, which is one of the most promising techniques for high quality semiconductor applications.[4] ZnO and In_2O_3 are typical high performance transparent conductive films which can be deposited by FCVA at low temperature. The optimized polycrystalline indium-tin-doped oxide (ITO) film fabricated on Si (111) substrate by FCVA below 350 °C has a high transmittance of 95% in the visible light region, the resistivity is 6.6×10^{-4} Ω·cm and electron carrier concentration is as high as 1.6×10^{21} cm^{-3}.[5] FCVA technique can cause high temperature in the film surface and high growth rate and high quality crystal growth. Using this technique, 500 nm–1300 nm thick and high transparent ZnO:Al films were grown on glass at room temperature (RT) with rates exceeding 250 $nm{\cdot}min^{-1}$ while maintaining resistivity below 5×10^{-4} Ω·cm with electron mobility as high as 60 $cm^2/V{\cdot}s$.[6]

Mixing ZnO in BTO can maintain BTO's mobility and improve its stability when deposited at low temperature.[7] Indium (In) is usually used as a substituting element for Sn in BTO compound. The induced ferromagnetism and enhanced optical behavior in indium-doped BTO system had been reported due to the relatively non-toxic, easily fusible nature and high mobility, trapping and electron generation rate for In.[8] The photocatalytic efficiency of BTO can be enhanced by In doping as a result of its capability to hinder the electron–hole recombination.[9] Indium is usually used in acceptor substituted $BaSn_{1-x}In_xO_{3-y}$ proton conductors.[10–12] In-substituted BTO ($BaSn_{1-x}In_xO_{3-y}$, $x=0.125$, 0.25, and 0.50) compounds were prepared by a gel polymerization method. All compounds were single-phase perovskite structure. The highest proton conductivity of 9.5×10^{-4} S/cm was obtained for $BaSn_{0.5}In_{0.5}O_{2.75}$.[12]

However, there are few reports about the optical and electrical properties of In_2O_3 mixed BTO films. With the ener-

†Corresponding author. E-mail: yaojk@m.scnu.edu.cn

© 2023 Chinese Physical Society and IOP Publishing Ltd

getic FCVA technique the poly-crystalline BTO phase can be synthetized at low temperature with improved properties while there are no reports till now. In the article, the microstructure, optical and electrical properties of In_2O_3 mixed BTO films deposited by FCVA technique at RT were investigated.

2. Experiment

The BITO films were deposited by FCVA technique at RT. A cylindrical 80-wt% BTO and 20-wt% In_2O_3 mixed target in diameter of 60 mm and thickness of 5 mm was mounted on a water-cooled copper plate. Typically, the base vacuum of the chamber was 2×10^{-6} Torr (1 Torr = 1.33322×10^{2} Pa) by a two-stage pumping system made of a mechanical roughening pump and a cryogenic pump. The pressure during the deposition was increased to 2×10^{-4} Torr due to the injection oxygen gas into the chamber. The oxygen gas was introduced into the chamber directly by a mass flow controller with constant flow rate of 50 sccm. The substrates were K9 glasses of thickness of about 1 mm. Prior to loading into the chamber, the substrates were cleaned by ultrasonic bath in acetone, isopropyl alcohol, and rinsed in de-ionized water, and then dried by nitrogen gas. The arc current of 100 A was used for the sample. A toroidal magnetic field around 40 mT was employed to produce the axial and curvilinear fields to steer the plasma.

The structure of film was studied by a Rigaku x-ray diffraction (XRD) meter. The x-ray source used is Cu $K\alpha$ radiation at wavelength of 0.15418 nm. The surface morphology of film was studied by a ZEISS Gemini scanning electron microscope (SEM). A Lambda 900 spectrometer was used to measure the transmittance and reflectance of film. To determine the optical constants and thickness of film the Spectroscopic Ellipsometer (SE, Semilab GES5-E) was used. The carrier transportation properties of film was obtained by a Hall system using the van der Pauw configuration (HMS 2000) at RT.

3. Results and discussion

The crystalline phase and crystal orientation are evaluated using XRD. Figure 1 shows the XRD pattern of BITO film on glass substrate. The XRD pattern indicate that the film exhibit a polycrystalline body-centered cubic crystal structure ($a = b = c = 1.0118$ nm) of In_2O_3 clearly. Four peaks appear at $2\theta = 30.6°$, 35.4°, 50.9°, and 60.6° which correspond to the (222), (400), (440), and (622) directions of the body-centered cubic crystal structure of In_2O_3 (referred from In_2O_3 XRD standard card number PDF#06-0416). The film also has a polycrystalline perovskite structure of BTO. Peaks appear at $2\theta = 24.2°$, 30.6°, 36.4°, 47.9°, 58.6°, 76.0°, 82.0°, and 89.0° which correspond to the (001), (011), (111), (002), (112), (103), (222), and (213) directions of the perovskite crystal structure of BTO (referred from BTO XRD standard card number PDF#15-0780). The peaks intensity of In_2O_3 are sharp than those of BTO due to its poor crystalline. This is the first time the BTO crystalline has appeared in film on glass substrate when deposited at RT by previously reported fabricating techniques due to the high energy of FCVA. The result indicate that the film has two single phase of In_2O_3 and BTO and no other mixed compound has been found. Figure 2 shows the surface morphology of BITO film by SEM. Clear polycrystalline with grain size below 200 nm has been found which is consistent with the XRD result.

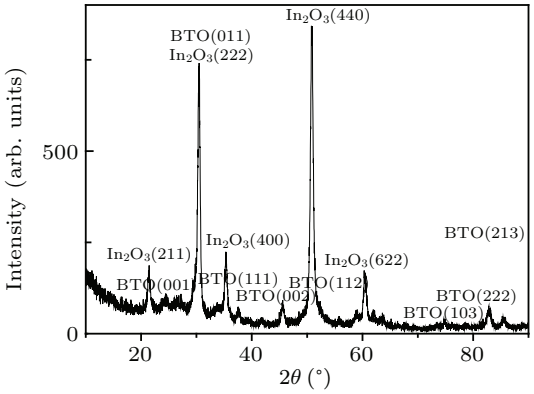


Fig. 1. XRD pattern of BITO film.

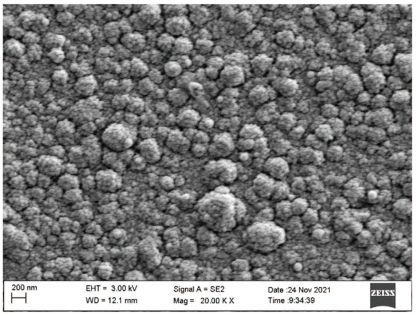


Fig. 2. The surface morphology of BITO film.

The transmittance and reflectance spectra of BITO film on glass substrate from wavelength of 300 nm to 2000 nm are shown in Fig. 3. The overall transmittance of the film is in 70%–85% in the wavelength range of 550 nm–800 nm. The overall reflectance of the film is below 35% in the whole wavelength range. The transmittance and reflectance vary not apparently in the near infrared wavelength range due to the low electron carrier concentration in film as listed below. The absorption of film is calculated by $A = 1 - T - R$, which sharply decreases from 300 nm indicating the absorption edge is at approximately 300 nm for the cut-off property at ultraviolet wavelength of transparent conductive film. The carrier electron concentration in film at RT tested by Hall system is 1.6×10^{19} cm^{-3}, which is larger than the effective density of states (4×10^{18} cm^{-3}) in conduction band at RT. This causes electrons fulfill at the low energy levels in conduction band and photons with energy larger than the intrinsic band gap be absorbed. The absorption decreases to zero above 600 nm.

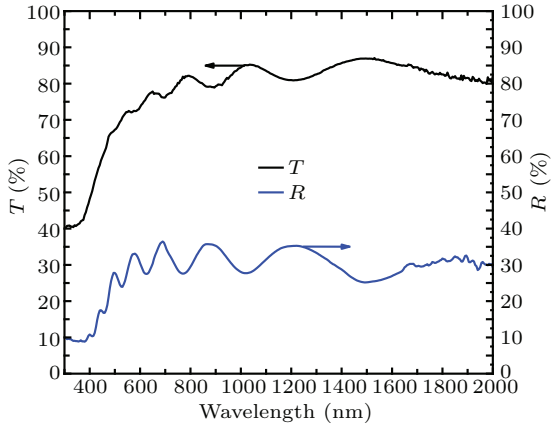


Fig. 3. The transmittance and reflectance spectra of BITO film.

The linear refractive index (N_1), extinction coefficients (K) and film thickness of BITO are measured by SE method. The film has thickness of 300 nm. The N_1 and K are shown in Fig. 4(a). The real and imaginary components of the dielectric constants ε_1 and ε_2 are calculated by $(N_1 + \mathrm{i}K)^2 = \varepsilon_1 + \mathrm{i}\varepsilon_2$, as shown in Fig. 4(b). Figure 4(c) shows the cole–cole plots, from which the high frequency dielectric constant ε_∞ is determined at the interception of the real axis. The absorption coefficient α is calculated by $\alpha = 4\pi K/\lambda$, as shown in Fig. 4(d). It is known that the exponential optical energy dependence of α near the band gap can be described by $\alpha \propto \exp(E/E_\mathrm{u})$, where E is the photon energy and E_u is the Urbach energy related to the joint density of states determined by both conduction and valence band tail states. The extracted E_u is 32 meV. The indirect gap is determined by constructing Tauc plots of $(\alpha h\nu)^{1/2}$ *versus* $h\nu$. The resulting indirect gap is 2.7 eV, as seen in Fig. 4(e). The associated direct gap obtained from Tauc plot with $(\alpha h\nu)^2$ *versus* $h\nu$ is found to be 3.2 eV, as shown in Fig. 4(f). The spectral-dependent linear refractive index dispersion can be evaluated by the single effective-oscillator model proposed by Wemple–Didomenico.[13] The N_1 of the film can be related with oscillator energy (E_o) and dispersion energy (E_d) by the following equation:

$$N_1^2 - 1 = \frac{E_\mathrm{o}E_\mathrm{d}}{E_\mathrm{o}^2 - (h\nu)^2}, \tag{1}$$

where $h\nu$ is the photon energy, E_o and E_d are single oscillator constants. E_o is the average excitation energy for electronic transitions and E_d is the dispersion energy which is a measure of the strength of inter-band optical transitions. This model describes the dielectric response for transitions below the optical gap. It plays an important role in determining the behavior of N_1. Figure 4(g) shows the optical dispersion behavior of $(N_1^2 - 1)^{-1}$ *versus* $(h\nu)^2$ for the film. The oscillator parameters E_o and E_d are determined by fitting a straight line to the points. The slope of the linear relation represents $(E_\mathrm{o}E_\mathrm{d})^{-1}$ and the interception with the vertical axis equals $E_\mathrm{o}/E_\mathrm{d}$. The values of E_o and E_d are 3.5 and 2.9, respectively. The static refractive index N_s can be determined by $N_\mathrm{s} = (1 + E_\mathrm{d}/E_\mathrm{o})^{1/2} = 1.4$.[14] The static dielectric constant (ε_s) is estimated by $\varepsilon_\mathrm{s} = N_\mathrm{s}^2 = 1.8$. The refractive index can also be analyzed to determine the average oscillator wavelength (λ_0) and oscillator length strength (S_0) for the film. To obtain these values, the single term Sellmeier oscillator is used as[13]

$$n_1^2 - 1 = \frac{S_0\lambda_0^2}{1 - \lambda_0^2/\lambda^2}, \tag{2}$$

The λ_0 and S_0 values are obtained by the linear parts of $1/(N_1^2 - 1)$ *versus* λ^{-2}, as shown in Fig. 4(h), where $\lambda_0 = 375$ nm and $S_0 = 7.1 \times 10^{-6}$ nm^{-2}. It is known that the induced dielectric polarization (P) depends on the applied electrical field (E) which can be expressed in a series of powers of E by[15]

$$P = \chi^{(1)}E + \chi^{(2)}E^2 + \chi^{(3)}E^3, \tag{3}$$

where $\chi^{(1)}$, $\chi^{(2)}$, and $\chi^{(3)}$ represent the linear, second, and third-order nonlinear optical susceptibilities, respectively. The refractive index $N(\lambda)$ can be expressed as

$$N(\lambda) = N_1(\lambda) + N_2(\lambda), \tag{4}$$

where $N_1(\lambda)$ and $N_2(\lambda)$ are the linear and nonlinear refractive indexes. The $\chi^{(1)}$ is calculated by

$$\chi^{(1)} = (N_1^2 - 1)/4\pi. \tag{5}$$

The $\chi^{(3)}$ is calculated by

$$\chi^{(3)} = A[\chi^{(1)}]^4, \tag{6}$$

where A is equal to 1.7×10^{-10} esu. The N_2 is calculated by

$$N_2 = 12\pi\chi^{(3)}/N_1. \tag{7}$$

The $\chi^{(1)}$, $\chi^{(3)}$, and N_2 all follow the same variation trend of $N_1(\lambda)$ as shown in Figs. 4(i)–4(k).

The resistivity (ρ), mobility (μ), and electrical density (n) of the BITO film at RT are studied by Hall apparatus at RT. The van der Pauw technique in a magnetic field of 0.5 T is used to obtain the Hall constant R_H. The recorded resistance $R_\square$ is related to the resistivity ρ by $\rho = R_\square d$ where d is the film thickness. The conduction mobility μ can be found by $\mu = (\rho en)^{-1}$. The electron density is found from $n = f/eR_\mathrm{H}$ where f is a factor which depends on the type of scattering and the degree of degeneracy in the semiconductor. For complete degeneracy one may put $f = 1$. The sample is n-type with $R_\square = 704.7\ \Omega/\square$, $\rho \sim 0.02\ \Omega\cdot$cm, and $\mu \sim 18.9$ cm^2/V·s and $n \sim 1.6 \times 10^{19}$ cm^{-3}.

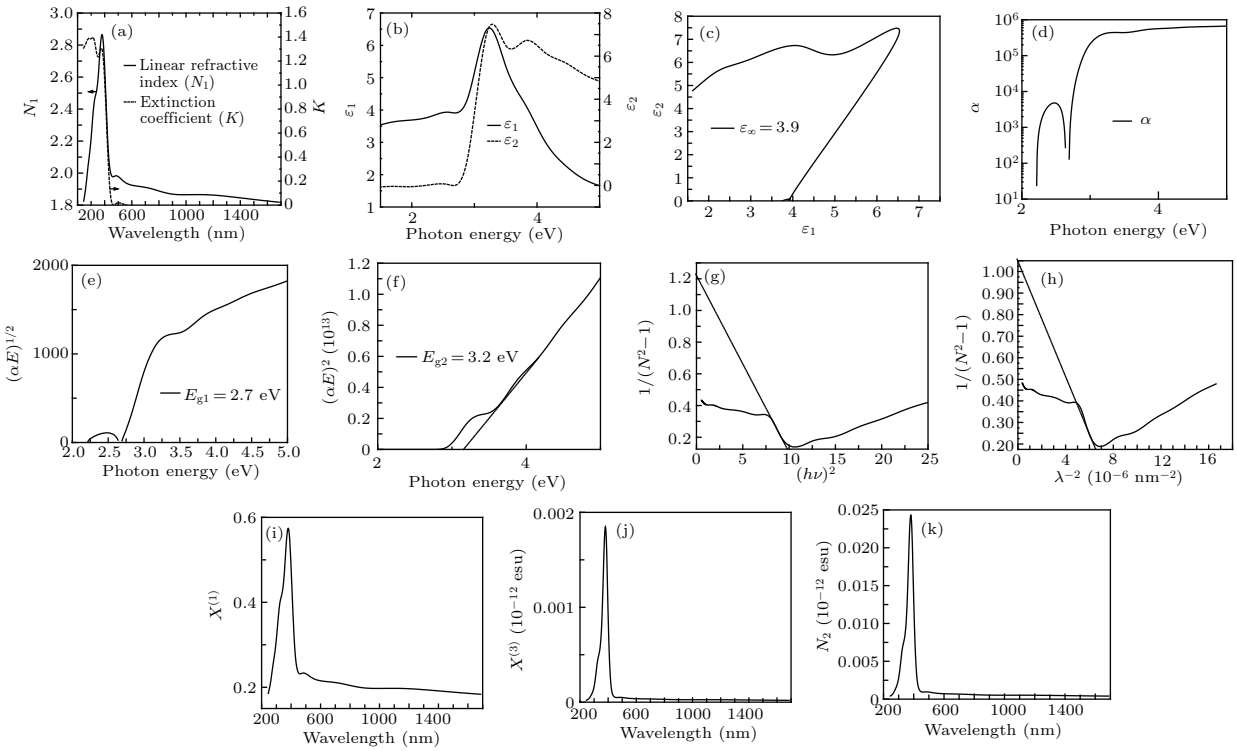


Fig. 4. (a) Linear refractive index and extinction coefficient, (b) real and imaginary parts of dielectric constants, (c) cole–cole plot of dielectric constants, (d) absorption coefficient, (e) indirect and (f) direct band gaps, (g) optical dispersion behavior $1/(N_1^2-1)$ *versus* $(h\nu)^2$, (h) optical dispersion behavior $1/(N_1^2-1)$ *versus* $(\lambda)^{-2}$, (i) linear nonlinear optical susceptibility, (j) third order nonlinear optical susceptibility, and (k) nonlinear refractive index of of BITO film.

4. Conclusion and perspectives

The BTO and In_2O_3 mixed film was first deposited by FCVA technique at RT. The structure, basic optical properties, and electrical properties of the film were studied. The film had isolated In_2O_3 and BTO polycrystalline phases, in which the polycrystalline BTO structure was first prepared at RT. The optical and electrical properties studied in this paper suggested that the BITO film fabricated by FCVA was a potential transparent conductor and can be used in low temperature device process. The results also indicated a new depositing technique of FCVA at RT for BTO-based transparent conductive film on glass substrate.

Acknowledgement

Project supported by the Enterprise Science and Technology Correspondent for Guangdong Province, China (Grant No. GDKTP2021015200).

References

[1] Lee W J, Kim H J, Kang J, Jang D H, Kim T H, Lee J H and Kim K H 2017 *Annu. Rev. Mater. Res.* **47** 391
[2] Prakash A and Jalan B 2019 *Adv. Mater. Interfaces* **6** 1900479
[3] Sriram S, Bhaskaran M, Mitchell D and Mitchell A 2010 *Cryst. Growth & Des.* **10** 761
[4] Tay B K, Zhao Z W and Chua D H 2006 *Mater. Sci. Eng. R* **52** 1
[5] Chen B J, Sun X W and Tay B K 2004 *Mater. Sci. Eng. B* **106** 300
[6] Mendelsberg R J, Lim S H, Zhu Y K, Wallig J, Milliron D J and Anders A 2011 *J. Phys. D: Appl. Phys.* **44** 232003
[7] Nahm H H, Kim H D, Park J M, Kim H S and Kim Y H 2020 *ACS Appl. Mater. Interfaces* **12** 3719
[8] Avinash M, Muralidharan M, Selvakumar S, Hussain S and Sivaji K 2020 *J. Mater. Sci. Mater. Electron.* **31** 3375
[9] Sobahi T R, Amin M S and Mohamed R M 2018 *Appl. Nanosci.* **8** 557
[10] Geneste G and Dezanneau G 2017 *Solid State Ion.* **308** 121
[11] Wang Y, Chesnaud A, Bevillon E, Yang J and Dezanneau G 2011 *Int. J. Hydrog. Energy* **36** 7688
[12] Wang Y, Chesnaud A, Bevillon E, Huang J and Yang J 2013 *Funct. Mater. Lett.* **6** 1350041
[13] Fung T C, Chuang C S, Nomura K, Shieh H P D, Hosono H and Kanicki J 2008 *J. Inform. Disp.* **9** 21
[14] Yakuphanoglu F, Cukurovali A and Yilmaz I 2004 *Physica B* **351** 53
[15] Yao J K, Ye F and Fan P 2020 *Chin. Phys. B* **29** 018105